Buckling and elastic stability of vertical ZnO nanotubes and nanorods

M. Riaz, A. Fulati, G. Amin, N. H. Alvi, O. Nur, and M. Willander

Citation: Journal of Applied Physics **106**, 034309 (2009); doi: 10.1063/1.3190481
View online: http://dx.doi.org/10.1063/1.3190481
View Table of Contents: http://scitation.aip.org/content/aip/journal/jap/106/3?ver=pdfcov
Published by the AIP Publishing

Buckling and elastic stability of vertical ZnO nanotubes and nanorods

M. Riaz,[a] A. Fulati, G. Amin, N. H. Alvi, O. Nur, and M. Willander
Department of Science and Technology, Campus Norrköping, Linköping University, SE-601 74 Norrköping, Sweden

(Received 15 February 2009; accepted 30 June 2009; published online 11 August 2009)

Buckling and elastic stability study of vertical well aligned ZnO nanorods grown on Si substrate and ZnO nanotubes etched from the same nanorods was done quantitatively by nanoindentation technique. The critical load, modulus of elasticity, and flexibility of the ZnO nanorods and nanotubes were observed and we compared these properties for the two nanostructures. It was observed that critical load of nanorods (2890 μN) was approximately five times larger than the critical load of the nanotubes (687 μN). It was also observed that ZnO nanotubes were approximately five times more flexible (0.32 nm/μN) than the nanorods (0.064 nm/μN). We also calculated the buckling energies of the ZnO nanotubes and nanorods from the force displacement curves. The ratio of the buckling energies was also close to unity due to the increase/decrease of five times for one parameter (critical load) and increase/decrease of five times for the other parameter (displacement) of the two samples. We calculated critical load, critical stress, strain, and Young modulus of elasticity of single ZnO nanorod and nanotube. The high flexibility of the nanotubes and high elasticity of the ZnO nanorods can be used to enhance the efficiency of piezoelectric nanodevices. We used the Euler buckling model and shell cylindrical model for the analysis of the mechanical properties of ZnO nanotubes and nanorods. © *2009 American Institute of Physics*. [DOI: 10.1063/1.3190481]

I. INTRODUCTION

ZnO is a noncentrosymmetric wurtzite structure material. The noncentrosymmetric behavior makes ZnO a piezoelectric material. ZnO piezoelectric thin films have been in use as a high frequency bulk acoustic wave and surface acoustic wave transducers and resonators.[1] Recently ZnO has attracted interest in the research community due to the availability at the low cost and excellent physical properties combined with the facilitated growth of its nanostructures. Wang and co-workers[2–4] made different piezoelectric nanogenerators from ZnO nanostructures. Mechanical characterization of ZnO nanostructures is then very important for the efficient operation of ZnO based nanopiezoelectric devices. Different metal and semiconductors nanorods/nanotubes were characterized for their mechanical properties.[5–14] In literature ZnO nanorods were also characterized for their mechanical and buckling properties.[15–25] Mostly for nanostructures grown in the vertical configuration (*c*-direction), the elastic stability of these structures is very important. Buckling is the measure of failure of the vertical structures. As ZnO nanorods were characterized for the buckling analysis, the ZnO nanotubes are not yet characterized for their buckling properties.

In this report we demonstrate nanoindentation experiments and analyze the elastic stability of the buckling failure and bending flexibility phenomena of vertical ZnO nanotubes and nanorods. We used the Euler buckling model for ZnO nanotubes/nanorods to calculate the Young modulus of elasticity, critical buckling stress, and critical strain of individual ZnO nanorods and nanotubes. Also we analyzed the ZnO nanotubes using the shell cylindrical model. The consistency between the predicted and the experimental results for critical load, stress, and strain was investigated.

II. EXPERIMENTAL

The ZnO nanorods used in the present experiment were grown on Si substrate by the aqueous chemical growth (ACG) method.[26] In the ACG method, zinc nitride dihydrate [$(Zn(NO_3)_2 6H_2O)$] was mixed with hexamethylenetetramine ($C_6H_{12}N_4$) using the same molar concentration for both solutions. The molar concentration was varied from 0.025*M* to 0.075*M*. The two solutions were stirred together and the substrates were placed inside the solution. Then, it was heated up to 90 °C for 3 h. Before the substrates were placed inside the solution, they were coated with a ZnO seed layer using the technique developed by Greene *et al.*[26] Zinc acetate dihydrate was diluted in ethanol to a concentration of 5 mM. Droplets of the solution were placed on the substrate until they completely covered the sample surface. After 10 s, the substrates were rinsed in ethanol and then dried in air. This procedure was repeated five times and then the samples were heated to 250 °C in air for 20 min to yield layers of ZnO on the substrates. The whole procedure was repeated twice in order to ensure a uniform ZnO seed layer. The side with the seed layer was mounted facing down in the solution. After the growth was completed, the samples were cleaned in de-ionized water and left to dry in air inside a closed beaker. ZnO nanotubes were obtained by etching the as grown ZnO nanorods. Elias *et al.*[27] explained the etching process and dissolution of the core of ZnO nanowires. After the growth of ZnO nanorods arrays, we divide the sample into two pieces. One piece was immersed in KCl solution of a con-

[a]Author to whom correspondence should be addressed. Electronic mail: riaz.muhammad@itn.liu.se.

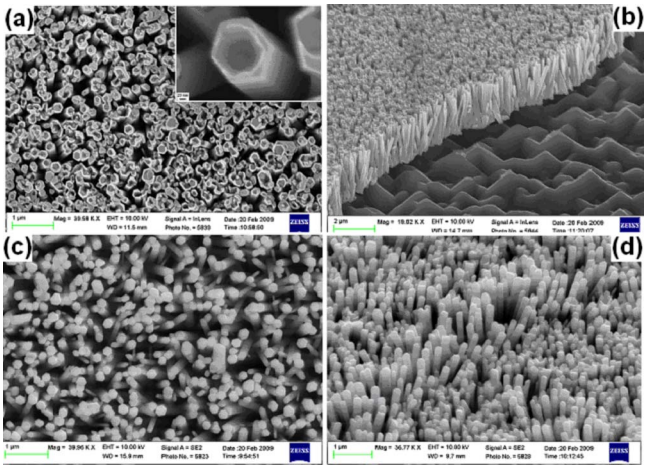

FIG. 1. (Color online) SEM images showing the morphologies of the as grown well aligned ZnO nanotubes and nanorods arrays. (a) and (b) and (c) and (d) are the top and side views of as etched nanotubes and nanorods, respectively. In (a) the *in situ* image of the tube has 20 nm scale bar, respectively.

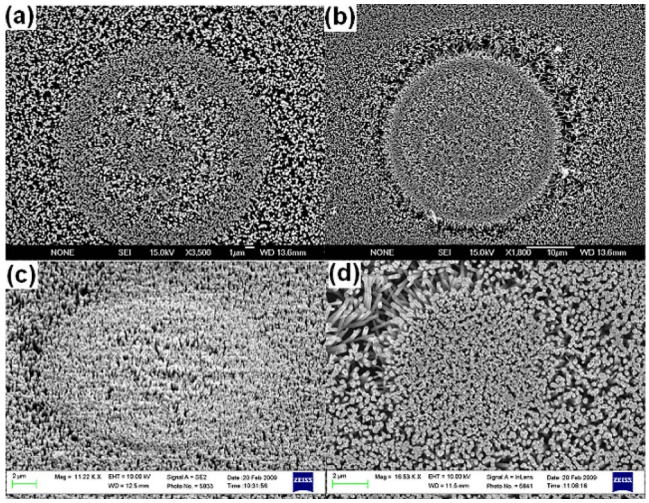

FIG. 2. (Color online) SEM images of the buckled ZnO nanorods and nanotubes arrays after nanoindentation. (a) and (b) and (c) and (d) are the buckled indentation images of ZnO nanorods and nanotubes, respectively.

centration in the range from 0.1*M* to 3.4*M* for time periods ranging from 3 to 17 h to obtain the ZnO nanotubes array. The temperature of the solution was kept at 95 °C. After 17 h of the immersion time in 3.0*M* KCl solution at 95 °C, we get tubular form of ZnO nanotubes array with good yield.

The surface morphology of the samples and size distribution of the nanorods/nanotubes were characterized by scanning electron microscope (SEM). X-ray diffraction (XRD) and energy dispersive x-ray spectroscopy (EDX) were also used to assess the structural properties. The buckling and instability behavior of the nanotubes and nanorods were investigated by means of Hysitron nanoindenter.

III. RESULTS AND DISCUSSION

Figure 1 show typical SEM images of the ZnO nanorods and the ZnO nanotubes etched from the as grown ZnO nanorods. Figures 1(a)–1(d) show top and side views of the ZnO nanorods/nanotubes arrays, respectively. The length, outside diameter and density of the nanorods and nanotubes are the same while the nanotubes have an inner diameter. From the SEM images the approximate outside diameter, inner diameter, length, and density were determined to be about 208 nm, 125 nm, 2219 nm, and 1.267×10^{9} cm^{-2}, respectively. It was found that the ZnO nanorods and nanotubes were distributed uniformly across the entire substrate. Figures 2(a)–2(d) show the SEM images of the ZnO nanorods and nanotubes after the buckling experiments. Figure 3 shows the measured XRD spectra of the samples. The peak originates at angles 34.32° and 34.84° in the spectra, which is an indication of the (0002) plane of ZnO nanorods and nanotubes, respectively. The XRD peaks of the ZnO (0002) plane show that the nanorods and the etched nanotubes were vertically grown and aligned along the *c*-axis direction and that they have good crystal quality. The XRD spectra also indicate that the angle of ZnO nanotubes shifted toward higher angles, indicating small plane displacement due to the residual compressive stresses which were developed in the nanotubes, may be due to the etching process. The residual compressive stresses may be the cause of reduced critical load for ZnO nanotubes. The chemical composition of ZnO nanorods and nanotubes were investigated by EDX analysis, as shown in Fig. 4. Figures 4(a) and 4(b) show the EDX analysis of ZnO nanorods and nanotubes, which indicate that the nanorods and nanotubes are composed of zinc and oxygen.

Vertical ZnO nanorods sample of 208 nm diameter and 2219 nm length was used in the nanoindentation experiment. The nanorods were loaded to a prescribed force and then unloaded in a force controlled mode. The nanorods were uniformly loaded and unloaded at a rate of 16 μN/s at room temperature. Figures 5(a) and 5(b) show the force displacement curve for the as grown ZnO nanorods. The nanorods were observed to be unstable at a load of 2890 μN, which is the average critical load of the nanorods, and the corresponding buckling energy was 2.6877×10^{-10} J. Similarly the ZnO nanotubes were loaded and unloaded the same way as the ZnO nanorods. The nanotubes were observed to be unstable at a load 687 μN, which is the average critical load of the nanotubes and its corresponding buckling energy was 7.557×10^{-11} J, respectively. Figures 6(a) and 6(b) show the force displacement curves of the ZnO nanotubes. Figures 5(a) and 6(a) show the buckled force displacement curves while Figs. 5(b) and 6(b) show the unbuckled and bending flexibility curves of the nanorods and nanotubes, respectively.

In Figs. 5(a) and 6(a), the loading portion consists of three main zones. The zone up to the critical point is categorized as the prebuckling zone, the buckled zone, and beyond the critical point is categorized as the postbuckling zone. In the prebuckling portion the data show a linear increase in the force with displacement, implying that the nanorods and nanotubes are vertically stable. In the buckled zone the vertical position of the nanorods and nanotubes is altered. The postbuckling category has many critical points 2, 3, 4, etc., and each critical point becomes a hinge for the next buckling of the nanorods and nanotubes. In this way a wave is generated along the nanorods/nanotubes length and thus the verti-

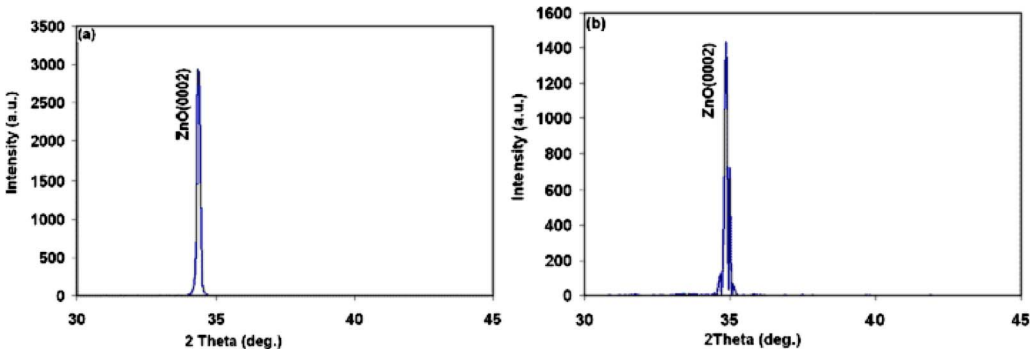

FIG. 3. (Color online) θ-2θ XRD of the as grown ZnO (a) nanorods and (b) nanotubes.

cal position of structure fails completely (collapses). In some cases this collapse is catastrophic and there is no alternative buckling points. Each alternative buckling failure stiffs the nanorods and a large amount of force is required than the preceded buckled situation. In the unloading portion of Figs. 5(a) and 6(a), we see no pop-in and pop-out indicating that there is no interaction between the nanorods/nanotubes and the indenter tip. This shows that the nanotubes/nanorods were broken and lost the elasticity behavior.

By comparing the critical load, the ZnO nanorods have a larger critical force, approximately five times more than the ZnO nanotubes etched from the same nanorods. This difference in critical load is due to (1) as tubular structures are more fragile than the solid structures, and because tubular structures have more porosity than the solid structures. (2) In Euler model the critical load is mainly dependent on the second moment of inertia, I, which is equal to $\pi D^4/64$ for the solid object while in shell cylindrical model for nanotubes it is dependent on the thickness of the nanotube. The diameter of the solid nanorod is usually larger than the thickness of the hollow nanotube, which can also further contribute to the reduction of the critical load of the nanotubes when compared to the nanorods. (3) As we etched chemically the nanotubes from the same nanorods, etching is not uniform and it leaves the inside surface of the nanotubes uneven and have some defects and kinks. These defects and kinks are more sensitive to buckling, making the nanotubes more fragile as compared to the solid nanorods. This is also seen from the force displacement curves. The force displacement curve of the nanorods gives more prominent waves after buckling while for the nanotubes there are fewer waves and is more sudden and catastrophic. Finally (4), the indenter tip interaction with the solid uniform surface and hollow uneven surface may also contribute to the reduction of the nanotube critical load compared to the solid nanorod.

Figures 5(b) and 6(b) show the bending flexibility of the same samples. In this experiment the nanorods/nanotubes were loaded and unloaded in the same rate as in Figs. 5(a) and 6(a) but only up to near the approximate first critical point. The curves are very symmetrical which show that during loading the indenter tip exert a constant force on the nanorods/nanotubes while during unloading the nanorods/nanotubes exert approximately the same force on the indenter tip due to the elastic behavior of the structure. The unloading force on the indenter is applied by the transducer and the elastic behavior of the nanotubes/nanorods. During this test we did not observe any critical point. As our Hysitron nanoindenter is equipped with atomic force microscope, before the indentation we scanned the sample and focused on a specific area. By performing the indentation experiment the scanning of the sample is stopped. First we performed the bending test and then keep the same scanning area, only increasing the load in the transducer unit to perform the buckling test on the same area. The force displacement curves also show that the displacement is more for the nanotubes than for the solid nanorods. From Figs. 5 and 6 we observed that the ZnO nanotubes were approximately five times more flexible (0.32 nm/μN) than the nanorods (0.064 nm/μN). This is because the nanotubes have larger surface area and high porosity. This flexibility of the nanotubes is very important as it can enhance the efficiency of piezoelectric nanodevices.

The behavior of an ideal column under axial compres-

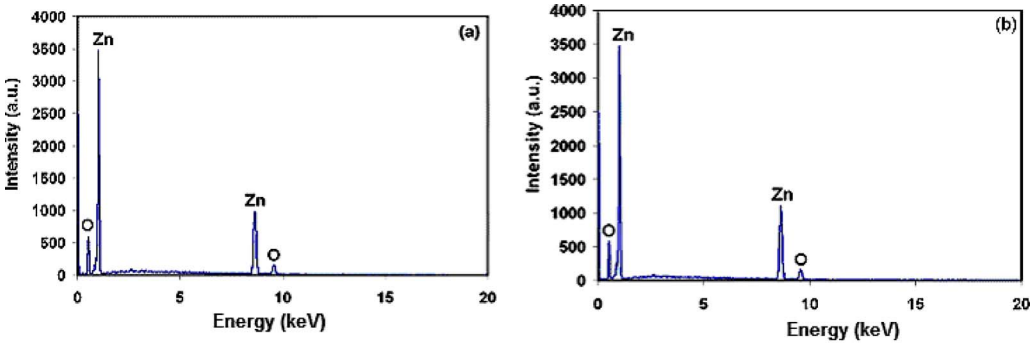

FIG. 4. (Color online) EDX spectra of ZnO (a) nanorods and (b) nanotubes.

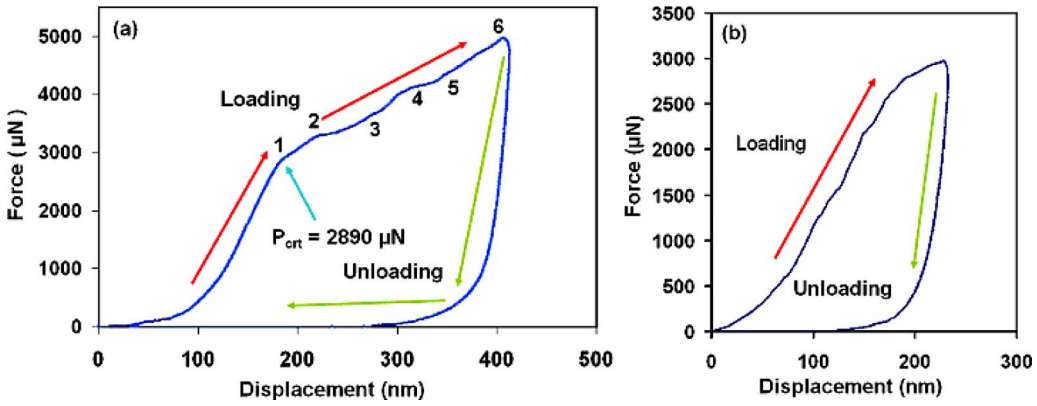

FIG. 5. (Color online) Load vs displacement curve of the as grown ZnO nanorods from indentation experiment, (a) buckled ZnO nanorods, and (b) bending flexibility of ZnO nanorods curve.

sive load can be summarized as follows: if the load P is less than the critical load P_{crt}, the nanorods are in stable equilibrium, also if the load P is equal to the critical load P_{crt}, the nanorods are in neutral equilibrium, and if the load P is greater that the critical load P_{crt}, the nanorods are in an unstable equilibrium.[28] Our nanorods and nanotubes are long; the nanorods will be analyzed using the Euler model while the nanotubes will be analyzed by using the Euler as well as the shell cylindrical model.

The general form of the Euler equations for a straight column under uniaxial compression is[28]

$$P_{crt} = \frac{C\pi^2 EI}{L^2}, \tag{1}$$

where C is the end condition of the column, and it has different values which are given in Table I. P_{crt} is the critical load, E is Young's modulus of elasticity, L is the length, and I is the moment of inertia and equal to $\pi D^4/64$ for solid nanorod and $(\pi/64)(D_o^4 - D_i^4)$ for hollow nanotubes. Here D_o is the outside diameter and D_i is the inner diameter of the nanotube. Also $\pi D^2/4$ and $(\pi/4)(D_o^2 - D_i^2)$ represent the area of the ZnO nanorods and the nanotubes, respectively.

The diamond tip used is of a conical shape and is 10 μm in radius, but the actual radius may be different than the registered on the tip. Figure 2 shows the tip indentation area on ZnO nanorods and nanotubes samples. The indentation area on ZnO nanorods and nanotubes may be different due to the flexibility behavior of the nanostructures. As the ZnO nanotubes have more flexibility than the nanorods, thus the indentation area on ZnO nanotubes may be less than the indentation area on ZnO nanorods. The approximate actual tip radius is about 17.5 μm and show spherical behavior instead of conical. So approximately 12 696 nanorods and nanotubes were loaded axially, and thus the average buckling loads of the individual ZnO nanorod or nanotube are approximately 0.23 and 0.0541 μN, respectively. In our earlier work on buckling characterization of ZnO nanorods grown by the same method, the critical load for the nanorods is very similar to the present experiment,[15] implying that our buckling characteristics results are consistent and reliable.

In Figs. 5(a) and 6(a) considering the prebuckling portion of the curves, the load is almost linear up to the first critical point, i.e., point 1. In this region we assume that the linear elasticity theory is applicable. Thus the stress is directly proportional to the strain,

$$\sigma_c = E\varepsilon_c, \tag{2}$$

$$\sigma_c = \frac{P_{crt}}{A}, \tag{3}$$

where σ_c and ε_c are the critical stress and critical strain.

According to the shell cylindrical theory,[29] if $(\pi R/L)^2$ is less than $2R\sqrt{3(1-\nu^2)}/t$ then the cylindrical tube will be

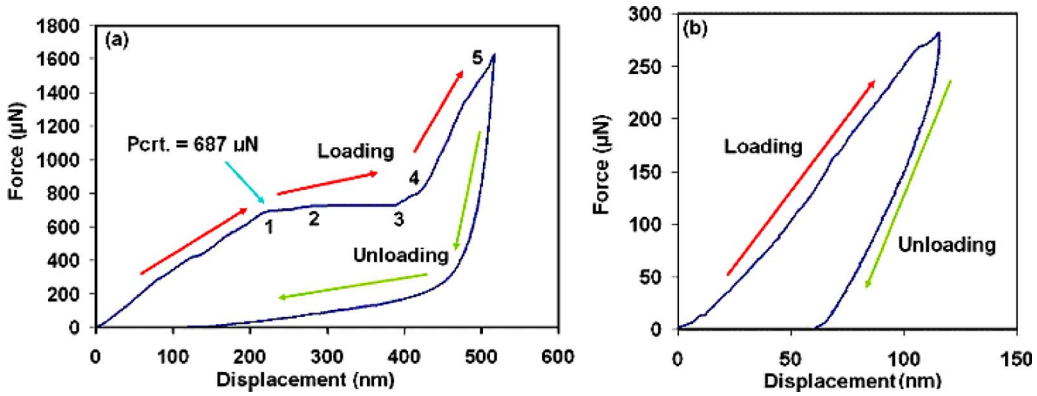

FIG. 6. (Color online) Load vs displacement curve of the etched ZnO nanotubes from the nanoindentation experiment, (a) buckled ZnO nanotubes, and (b) bending flexibility of ZnO nanotubes curve.

TABLE I. Displays, critical stress, buckling strain, and modulus of elasticity for the ZnO nanorods and nanotubes.

End condition of nanowire	C	Modulus of elasticity (GPa)		Critical stress (MPa)		Critical strain (%)		Analysis model
		Nanorod	Nanotube	Nanorod	Nanotube	Nanorod	Nanotube	
Fixed-free	0.25	5.0	1.351	6.765	2.5	0.135	0.185	Euler
Pinned-pinned	1.00	1.25	0.338	6.765	2.5	0.540	0.74	
Fixed-pinned	2.00	0.625	0.169	6.765	2.5	1.08	1.48	
Fixed-fixed	4.00	0.3125	0.0845	6.765	2.5	2.16	2.96	

considered as long and the following equation can be used for predicting the critical strain, stress, and critical load:[29]

$$\varepsilon_{\mathrm{crt}} = \frac{t}{R\sqrt{3(1-\nu^2)}}, \tag{4}$$

$$\sigma_{\mathrm{crt}} = \frac{Et}{R\sqrt{3(1-\nu^2)}}, \tag{5}$$

$$P_{\mathrm{crt}} = 2\pi R t \sigma_{\mathrm{crt}} = \frac{2\pi E t^2}{\sqrt{3(1-\nu^2)}}, \tag{6}$$

where R, t, and ν are the outside radius, thickness, and Poisson's ratio of ZnO nanotubes. Similarly the length categorization is made for the ZnO nanorods in Ref. 28 and our nanorods are long and we will use Eq. (1) for further analysis. Equation (1) is the Euler buckling model in which the critical load depends on the length and radius of the nanorod/nanotube but in the shell cylindrical model, it is independent of length and radius and mainly dependent on the wall thickness of the shell. Equations (4)–(6) are based on the shell cylindrical model. It gives us the predicted critical load and strain in our nanotube samples. The elastic constants of ZnO nanotubes are taken from Ref. 30. The predicted critical load and strain are 720 μN and 23.88%, respectively. Our experimental values of critical load and strain are much less than the predicted one. The predicted values are overestimated due to Young's modulus of elasticity (E). As buckling is a structural failure phenomena and not a material failure phenomena, E has thus different values for different structures. If we assumed that both ends of the nanorods and nanotubes are fixed and use the value of E in Eq. (6), the predicted critical load then becomes 2.0 μN. Still this value is larger than the experimental value. To explicitly understand the buckling of ZnO nanotubes there is a need of a fundamental study by molecular dynamic simulation or by first principle atomic level simulation. Another main reason for this is that as our ZnO nanotubes are very thick, i.e., the ratio of t/R is very large that it will give us a higher predicted value. The shell cylindrical theory is very appropriate for smaller and thin wall tubes. Both of our ZnO nanorod and nanotubes are long and the nanotubes have a thicker wall. We then used Eqs. (1)–(3) of the Euler buckling model to calculate Young's modulus of elasticity, critical stress, and strain. As shown in Table I, we determined the modulus of elasticity (E) of the ZnO nanorods/nanotubes and the corresponding buckling stress (σ_c) and strain (ε_c) for different end conditions of the nanorods.

IV. CONCLUSION

In this paper we demonstrated the experimental observation of the instability and buckling characterization of well aligned single crystal ZnO nanotube/nanorods grown by using the low temperature chemical growth approach on a Si substrate. The critical buckling loads of the ZnO nanorods and nanotube are found to be 2890 and 687 μN and their corresponding buckling energies are 2.6877×10^{-10} and 7.557×10^{-11} J, respectively. The approximate critical load bore by a single ZnO nanorod and nanotube are also calculated to be 0.23 and 0.0541 μN. It is concluded that the ZnO nanotubes are more fragile and flexible, very sensitive to axial loading than solid nanorods. We have used the Euler model for the nanorods and nanotubes for the evaluation of Young's modulus of elasticity and the critical strain of single ZnO nanorod/nanotube for different end conditions. The shell cylindrical buckling model was also used for the analysis of ZnO nanotubes. It was observed that the calculated critical stress and strain by using the shell cylindrical model were much larger than the experimental values. It was also observed that the ZnO nanotubes are approximately five times more flexible than the nanorods. This flexibility is very important as it can enhance the efficiency of piezoelectric nanodevices.

[1] F. S. Hickernell, Proc.-IEEE Ultrason. Symp. **1996**, 235.
[2] Z. L. Wang and J. H. Song, Science **312**, 242 (2006).
[3] R. Yang, Y. Qin, L. Dai, and Z. L. Wang, Nat. Nanotechnol. **4**, 34 (2009).
[4] X. Wang, J. Song, J. Liu, and Z. L. Wang, Science **316**, 102 (2007).
[5] L. T. Ngo, D. Almecija, J. E. Sader, B. Daly, N. Petkov, J. D. Holmes, D. Erts, and J. J. Boland, Nano Lett. **6**, 2964 (2006).
[6] X. Tao and X. Li, Nano Lett. **8**, 505 (2008).
[7] J. Biener, A. M. Hodge, J. R. Hayes, C. A. Volkert, L. A. Zepeda-Ruiz, A. V. Hamza and F. F. Abraham, Nano Lett. **6**, 2379 (2006).
[8] Q. Xiong, N. Duarte, S. Tadigadapa and P. C. Eklund, Nano Lett. **6**, 1904 (2006).
[9] B. Wu, A. Heidelberg, and J. J. Boland, Nano Lett. **6**, 468 (2006).
[10] X. Li, X. Wang, and P. C. Eklund, Nano Lett. **5**, 1982 (2005).
[11] A. Heidelberg, L. T. Ngo, B. Wu, M. A. Phillips, S. Sharma, T. I. Kamins, J. E. Sader, and J. J. Boland, Nano Lett. **6**, 1101 (2006).
[12] G. Stan, C. V. Ciobanu, P. M. Parthangal, and R. F. Cook, Nano Lett. **7**, 3691 (2007).
[13] S. C. Hung, Y. K. Su, T. H. Fang, S. J. Chang, and L. W. Ji, Nanotechnology **16**, 2203 (2005).
[14] J. F. Waters, P. R. Guduru, M. Jouzi, J. M. Xu, T. Hanlon, and S. Suresh, Appl. Phys. Lett. **87**, 103109 (2005).
[15] M. Riaz, O. Nur, M. Willander, and P. Klason, Appl. Phys. Lett. **92**, 103118 (2008).

[16]M. Riaz, A. Fulati, Q. X. Zhao, O. Nur, M. Willander, and P. Klason, Nanotechnology **19**, 415708 (2008).
[17]M. Riaz, A. Fulati, L. L. Yang, O. Nur, M. Willander, and P. Klason, J. Appl. Phys. **104**, 104306 (2008).
[18]G. Feng, W. D. Nix, Y. Yoon, and C. J. Lee, J. Appl. Phys. **99**, 074304 (2006).
[19]A. V. Desai and M. A. Haque, Sens. Actuators, A **134**, 169 (2007).
[20]J. Song, X. Wang, E. Riedo, and Z. L. Wang, Nano Lett. **5**, 1954 (2005).
[21]M. Lucas, W. Mai, R. Yang, Z. L. Wang, and E. Riedo, Nano Lett. **7**, 1314 (2007).
[22]C. Q. Chen and J. Zhu, Appl. Phys. Lett. **90**, 043105 (2007).
[23]S. J. Young, L. H. Ji, S. J. Chang, T. H. Fang, T. J. Hsueh, T. H. Meen, and I. C. Chen, Nanotechnology **18**, 225603 (2007).
[24]L. W. Ji, S. J. Young, T. H. Fang, and C. H. Liu, Appl. Phys. Lett. **90**, 033109 (2007).
[25]S. O. Kucheyev, J. E. Bradby, J. S. Williams, C. Jagadish, and M. V. Swain, Appl. Phys. Lett. **80**, 956 (2002).
[26]L. Greene, M. Law, D. Tan, M. Montano, J. Goldberger, G. Somorjai, and P. Yang, Nano Lett. **5**, 1231 (2005).
[27]J. Elias, R. T. Zaera, G. Y. Wang, and C. L. Clement, Chem. Mater. **20**, 6633 (2008).
[28]J. E. Shigley, C. R. Mischke, and R. G. Budynas, *Mechanical Engineering Design*, 7th ed. (McGraw-Hill, New York, 2004).
[29]S. P. Timoshenko and J. M. Gere, *Theory of Elastic Stability*, 2nd ed. (McGraw-Hill, New York, 1961).
[30]Y. Peng-Fei, D. Ze-Jun, and J. Xin, Chin. Phys. Lett. **25**, 1030 (2008).